© 2019. Published by The Company of Biologists Ltd | Development (2019) 146, dev168120. doi:10.1242/dev.168120

STEM CELLS AND REGENERATION

RESEARCH ARTICLE

Ecrg4 deficiency extends the replicative capacity of neural stem cells in a Foxg1-dependent manner

Yuka Nakatani[1], Hiroshi Kiyonari[2] and Toru Kondo[3,*]

ABSTRACT

The self-renewal activity of neural stem cells (NSCs) has been suggested to decrease with aging, resulting in age-dependent declines in brain function, such as presbyopia and memory loss. The molecular mechanisms underlying decreases in NSC proliferation with age need to be elucidated in more detail to develop treatments that promote brain function. We have previously reported that the expression of esophageal cancer-related gene 4 (*Ecrg4*) was upregulated in aged NSCs, whereas its overexpression decreased NSC proliferation, suggesting a functional relationship between Ecrg4 and NSC aging. Using Ecrg4-deficient mice in which the *Ecrg4* locus was replaced with the *lacZ* gene, we here show that Ecrg4 deficiency recovered the age-dependent decline in NSC proliferation and enhanced spatial learning and memory in the Morris water-maze paradigm. We demonstrate that the proliferation of Ecrg4-deficient NSCs was partly maintained by the increased expression of Foxg1. Collectively, these results determine Ecrg4 as a NSC aging factor.

KEY WORDS: Ecrg4, Neural stem cells (NSCs), Foxg1, Aging, Memory

INTRODUCTION

Tissue-specific stem cells have been suggested to self-renew throughout the life of an animal and give rise to the many differentiated cells required to maintain tissue homeostasis and repair damaged tissues (Goodell et al., 2015; Krieger and Simons, 2015). However, stem cell proliferation declines with aging, resulting in defects in the residing tissue function, decreased tissue-repairing abilities and increases in the incidences of degenerative diseases (Fuchs and Chen, 2013; Krieger and Simons, 2015; Liu and Rando, 2011). Therefore, the molecular mechanisms responsible for stem cell aging need to be elucidated in more detail.

Esophageal cancer-related gene 4 (*Ecrg4*) was originally identified as one of the genes that are expressed at lower levels in esophageal cancer cells than in the surrounding non-cancer tissues (Su et al., 1998). Decreases in Ecrg4 expression were subsequently detected in various types of cancer tissues (Götze et al., 2009; Sabatier et al., 2011; Yue et al., 2003). While overexpression of Ecrg4 was found to prevent tumorigenesis by inhibiting cancer cell proliferation, it was revealed that Ecrg4 fragments secreted from cancer cells induced tumor eradication by activating both innate and adaptive immune system *in vivo* (Li et al., 2009, 2010; Moriguchi et al., 2016; Xu et al., 2013). Taken together, these findings indicated that Ecrg4 acts as a novel type of tumor suppresser.

We have independently identified Ecrg4 as a new cell senescence-associating factor; the expression of Ecrg4 was induced in senescent oligodendrocyte precursor cells (OPCs) that were cultured in the presence of high concentrations of fetal bovine serum, whereas its overexpression induced OPCs to become senescent with cell-cycle arrest, a large flat shape and senescence-associated β-galactosidase (β-gal) activity (Kujuro et al., 2010). We further demonstrated that some neural cells, including OPCs and neural stem cells (NSCs), in aged mouse brains were Ecrg4 positive, whereas this immunoreactivity was weaker in young brains (Kujuro et al., 2010). These findings suggested that Ecrg4 is involved in NSC aging *in vivo*.

In order to address this possibility, we generated *Ecrg4* knock-in (*Ecrg4KI*) mice by replacing the *Ecrg4* locus with the *lacZ* gene, and analyzed NSC functions. We herein demonstrate that *Ecrg4*-deficient NSCs maintained their proliferation activity during cultivation, even in the presence of serum that normally prevents NSC proliferation, and with age. Furthermore, the Morris water maze test revealed that spatial learning and memory were markedly better in *Ecrg4KI* mice than in wild-type mice. Taken together, these results determine Ecrg4 as a novel NSC-aging factor.

RESULTS

Ecrg4 is predominantly expressed in ependymal cells and NSCs

We replaced the first exon, which contains the first ATG codon on the *Ecrg4* locus, with a *floxed-lacZ* gene and generated $Ecrg4^{floxed\text{-}lacZ/+}$ (*Ecrg4hetero*) mice that developed normally and were fertile. We then crossed heterozygote mice and obtained $Ecrg4^{floxed\text{-}lacZ/floxed\text{-}lacZ}$ (*Ecrg4KI*) mice that were also viable and developed normally, indicating that Ecrg4 is not essential for development (Fig. S1).

We stained *Ecrg4hetero* mouse brains of 6 m and 15 m using X-gal and detected strong β-gal activity in the choroid plexus, which was consistent with previous findings (Gonzalez et al., 2011; Kujuro et al., 2010) and with data in the Allen Brain Atlas (www.brain-map.org) (Fig. 1A and Fig. S2A). We also observed $\beta\text{-gal}^{+}$ cells in the NSC niches, ependymal layer, ventricular zone/subventricular zone (VZ/SVZ) and dentate gyrus (DG) (Fig. 1A and Fig. S2A, I and II). We confirmed the Ecrg4 expression in these area by immunolabeling brain sections for Ecrg4 (Fig. S3). These results apparently indicated that Ecrg4 is expressed in the NSC niches.

To identify which cells in the ependymal layer and VZ/SVZ express β-gal, we immunolabeled brain sections from *Ecrg4KI* mice for β-gal and neural markers, and found that the β-gal-expressing cells in the ependymal layer were positive for nestin, glial fibrillary acidic protein (GFAP) and S100β (Fig. 1B-D and Fig. S2B)

[1]Division of Bio-Function Dynamics Imaging, Center for Life Science Technology, RIKEN, Kobe, Hyogo 650-0047, Japan. [2]Animal Resource Development Unit and Genetic Engineering Team, Center for Life Science Technology, RIKEN, Kobe, Hyogo 650-0047, Japan. [3]Division of Stem Cell Biology, Institute for Genetic Medicine, Hokkaido University, Sapporo 060-0815, Japan.

*Author for correspondence (tkondo@igm.hokudai.ac.jp)

T.K., 0000-0002-7755-2650

Received 21 May 2018; Accepted 28 January 2019

Development (2019) 146, dev168120. doi:10.1242/dev.168120

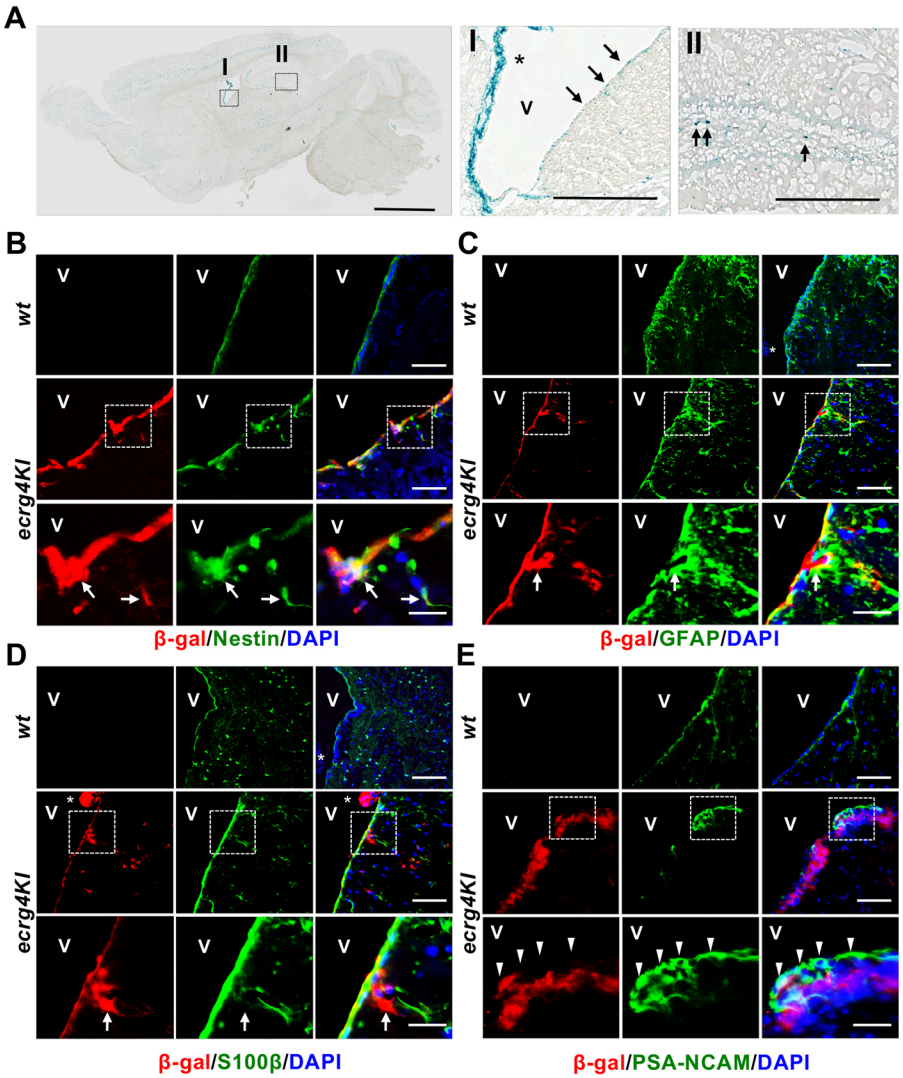

Fig. 1. Increased Ecrg4 promoter activity in the ventricular zone/subventricular zone, the ependymal cell layer and hippocampus. (A) X-gal staining (blue) of frozen brain sections of 6-month-old *Ecrg4KI* mice. High-magnification images are on the right: I, VZ/SVZ; II, DG. Arrows indicate X-gal$^+$ cells. Asterisk indicates the choroid plexus. (B-E) Immunostaining of brain sections of 6-month-old wild-type and *Ecrg4KI* mice for β-gal (red), which represents *Ecrg4* expression, and the neural markers (green) nestin (B), GFAP (C), S100β (D) and PSA-NCAM (E). Bottom row shows higher-magnification images of the boxed regions. Arrows show the cells leaving the VZ. Arrowheads show the developing neuronal precursor cells. Stars show the choroid plexus. All nuclei are counterstained with DAPI (blue). V, lateral ventricle. Scale bars: 2 mm in A; 200 µm and 50 µm (bottom row) in B-E.

(Doetsch et al., 1999; Steiner et al., 2007). A careful examination further revealed that Nestin$^+$ activated NSCs and GFAP$^+$ SVZ astrocytes, both of which are localized under the ependymal cell layer (Farkas and Huttner, 2008; Tramontin et al., 2003), were positive for β-gal (arrows in Fig. 1B,C). In contrast, migrating S100β$^+$ cells and polysialylated neural cell adhesion molecule (PSA-NCAM)$^+$ developing neuronal precursor cells were negative for β-gal (arrow and arrowheads in Fig. 1D and E, respectively). To further characterize β-gal$^+$ cells in the ependymal layer and VZ/SVZ, we dissected these areas from *Ecrg4hetero* mouse brains, purified β-gal$^+$ cells by flow cytometry (Fig. S4A), and then compared their gene expression profile with that of the cultured *Ecrg4hetero* NSCs. We found that β-gal$^+$ cells from the ependymal layer and VZ/SVZ were enriched in ependymal cells expressing connective tissue growth factor, vascular endothelial growth factor A, aquaporins, vimentin and *Foxj1*, while the cells also expressed NSC markers, *Foxg1*, *Notch* and prominin 1, more than in the cultured NSCs (Fig. S4B). It should be noted that *Ecrg4* expression was higher in cultured NSCs than that in β-gal$^+$ cells from the ependymal layer and VZ/SVZ, suggesting that *Ecrg4* expression was enhanced in the activated NSCs. Together, these results indicated that ependymal cells and activated NSCs express Ecrg4.

Ecrg4 deficiency prolongs NSC proliferation activity in the brain

There is much evidence that Ecrg4 prevents cell proliferation (Kujuro et al., 2010; Li et al., 2009, 2010; Xu et al., 2013). To examine the cell proliferation in the ependymal layer and VZ/SVZ cells, we immunolabeled sections of both wild-type and *Ecrg4KI* mouse brains at 6 months and 15 months for the proliferation marker Ki67 and nestin. The number of Ki67$^+$/nestin$^+$ cells in the ependymal layer and VZ/SVZ in wild-type mouse brains markedly decreased at 15 months (28 cells at 6 months versus one cell at 15 months), whereas a large number of nestin$^+$ cells were positive for Ki67 in the same aged *Ecrg4KI* mouse brains (32 cells at 6 months versus 14 cells at 15 months) (Fig. 2A, 6 m and Fig. 2B, 15 m). We also found Ki67$^+$/nestin$^+$ NSCs in the DG of 6-month-old *Ecrg4KI* mice (9 cells), but not in the same aged wild-type mice (Fig. 2C) or in the 15-month-old *Ecrg4KI* and wild-type mice (Fig. 2D). We confirmed that significant number of the cells in *Ecrg4KI* mouse ependymal layer, VZ/SVZ and DG were positive for another proliferation marker phosphorylated histone H3 at serine 10 (pH3 S10), compared with those in the same areas of the wild-type mouse (10 cells versus 1 cell in the ependymal layer and VZ/SVZ at 15 months; eight cells versus two cells in the DG at 6 months) (Fig. S5). We further found the increased number of

Development (2019) 146, dev168120. doi:10.1242/dev.168120

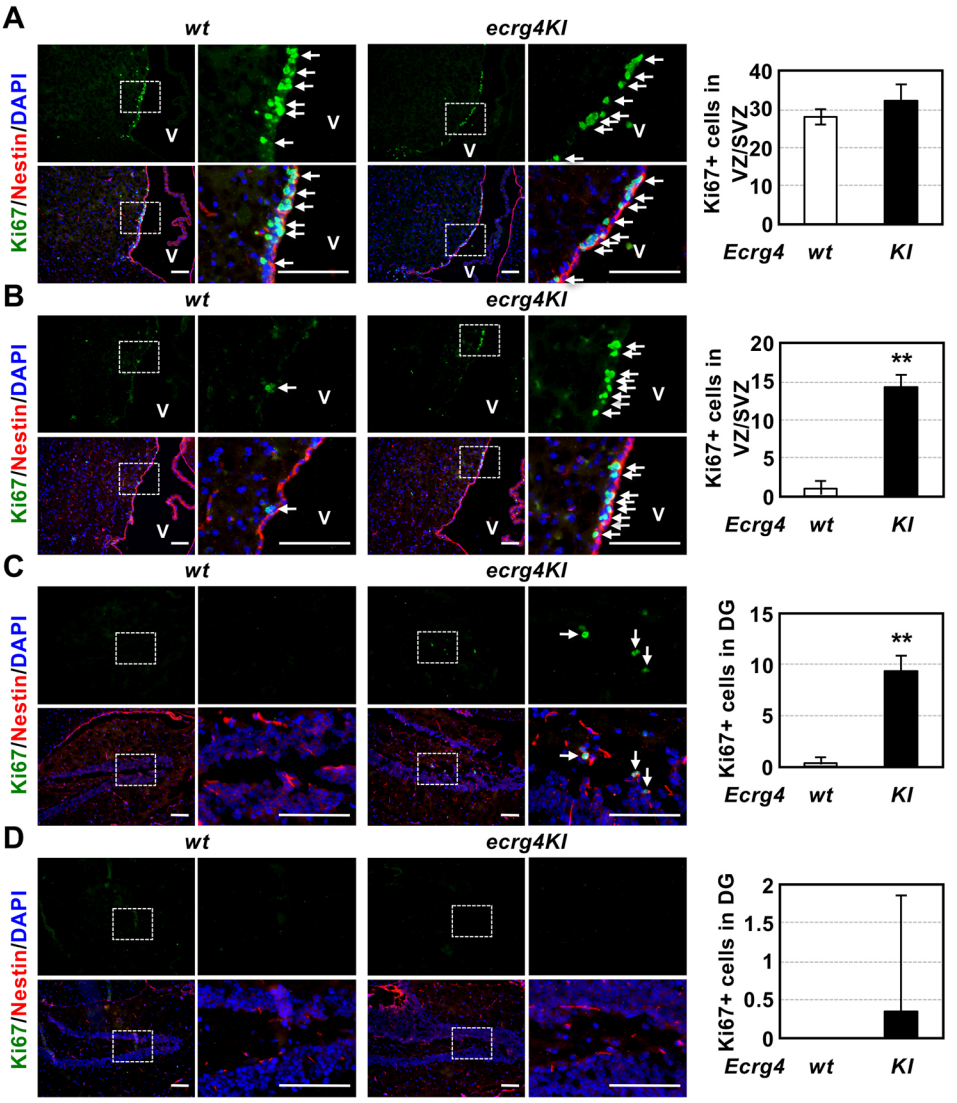

Fig. 2. *Ecrg4KI* mice retain proliferating NSCs longer than wild-type mice. Brain sections of wild-type and *Ecrg4KI* were immunolabeled for Ki67 (green) and nestin (red) to identify proliferating NSCs in the VZ/SVZ (arrows in A,B) and DG (arrows in C) of 6- (A,C) and 15-month-old (B,D) mice. Graphs show Ki67^{+} cell number in the VZ/SVZ (A,B) and DG (C,D). Data are mean±s.e.m. of three independent experiments. $^{**}P<0.01$. All nuclei are counterstained with DAPI (blue). Boxed areas are magnified in the panels on the right. V, lateral ventricle. Scale bars: 200 µm.

PSA-NCAM^{+} immature neurons in VZ/SVZ and DG of *Ecrg4KI*, compared with those in wild type (Fig. S6). Together, these findings indicated that Ecrg4 deficiency extends the proliferation activity of NSCs and keeps generating new neurons in the brain.

Ecrg4 deficiency maintains the proliferation activity of NSCs in a long-term culture

We investigated the molecular mechanism of how Ecrg4 deficiency keeps NSC proliferation. Ecrg4 was shown to induce the expression of pro-inflammatory cytokines, which prevent NSC proliferation, through the activation of a scavenger receptor/NF-κB signaling pathway in microglia (Lee et al., 2015; Kizil et al., 2015; Moriguchi et al., 2016, 2018). As cultured NSCs express both Ecrg4 and potential Ecrg4 receptors, including CD36 and Scarf1 (Fig. S4) (Moriguchi et al., 2018), secreted Ecrg4 may affect NSC proliferation in an autocrine/paracrine manner. To examine this possibility, we prepared three types of NSCs: *Ecrg4*$^{+/+}$, *Ecrg4*$^{+/-}$ and *Ecrg4*$^{-/-}$ cells, from wild type, *Ecrg4hetero* and *Ecrg4KI* embryonic brains, respectively. During culture, we noted that the proliferation of *Ecrg4*$^{+/-}$ and *Ecrg4*$^{-/-}$ cells was markedly faster than that of *Ecrg4*$^{+/+}$ cells. To quantify their proliferation activities, we performed a bromo-deoxyuridine (BrdU) incorporation assay. After 5 days in culture, 63% of *Ecrg4*$^{+/-}$ and 54% of *Ecrg4*$^{-/-}$ cells were positive for BrdU, whereas 29% of *Ecrg4*$^{+/+}$ cells were positive (Fig. 3A left panel). After 60 days in culture, *Ecrg4*$^{+/-}$ and *Ecrg4*$^{-/-}$ cells maintained higher proliferation activities than that of Ecrg4$^{+/+}$ cells (36% and 32% versus 8%, respectively) (Fig. 3A right panel), although the proliferation activities of all types of NSC appeared to decrease by 60 days. We also confirmed this tendency in the adult NSCs: adult *Ecrg4*$^{+/-}$ and *Ecrg4*$^{-/-}$ cells from 6-month-old VZ/SVZ and DG have proliferated faster than *Ecrg4*$^{+/+}$ cells from these areas (33% and 35% versus 19% in VZ/SVZ, 33% and 35% versus 19% in DG, respectively) (Fig. S7A,B).

We then addressed whether the secreted Ecrg4 affects NSC proliferation in an autocrine/paracrine manner. We cultured *Ecrg4*$^{-/-}$ cells with or without *Ecrg4*$^{+/+}$ cells for 7 days and then examined *Ecrg4*$^{-/-}$ cell proliferation using a BrdU incorporation assay. As shown in Fig. S7C, *Ecrg4*$^{-/-}$ cell proliferation significantly decreased when co-cultured with *Ecrg4*$^{+/+}$ cells, indicating that the secreted Ecrg4 inhibited *Ecrg4*$^{-/-}$ cell proliferation through its receptor(s) on the cells.

We analyzed the expression of cell-cycle regulators in *Ecrg4*$^{+/+}$, *Ecrg4*$^{+/-}$ and *Ecrg4*$^{-/-}$ cells, and their differentiation abilities. The expression of the cyclin-dependent kinase inhibitors (CDKIs) *p16*^{ink4a} (*Cdkn2a*), *p19*^{arf} and *p21*^{cip1} (*Cdkn1a*) was significantly low in 5-day-old cultured *Ecrg4*$^{-/-}$ cells, whereas the expression of

Development (2019) 146, dev168120. doi:10.1242/dev.168120

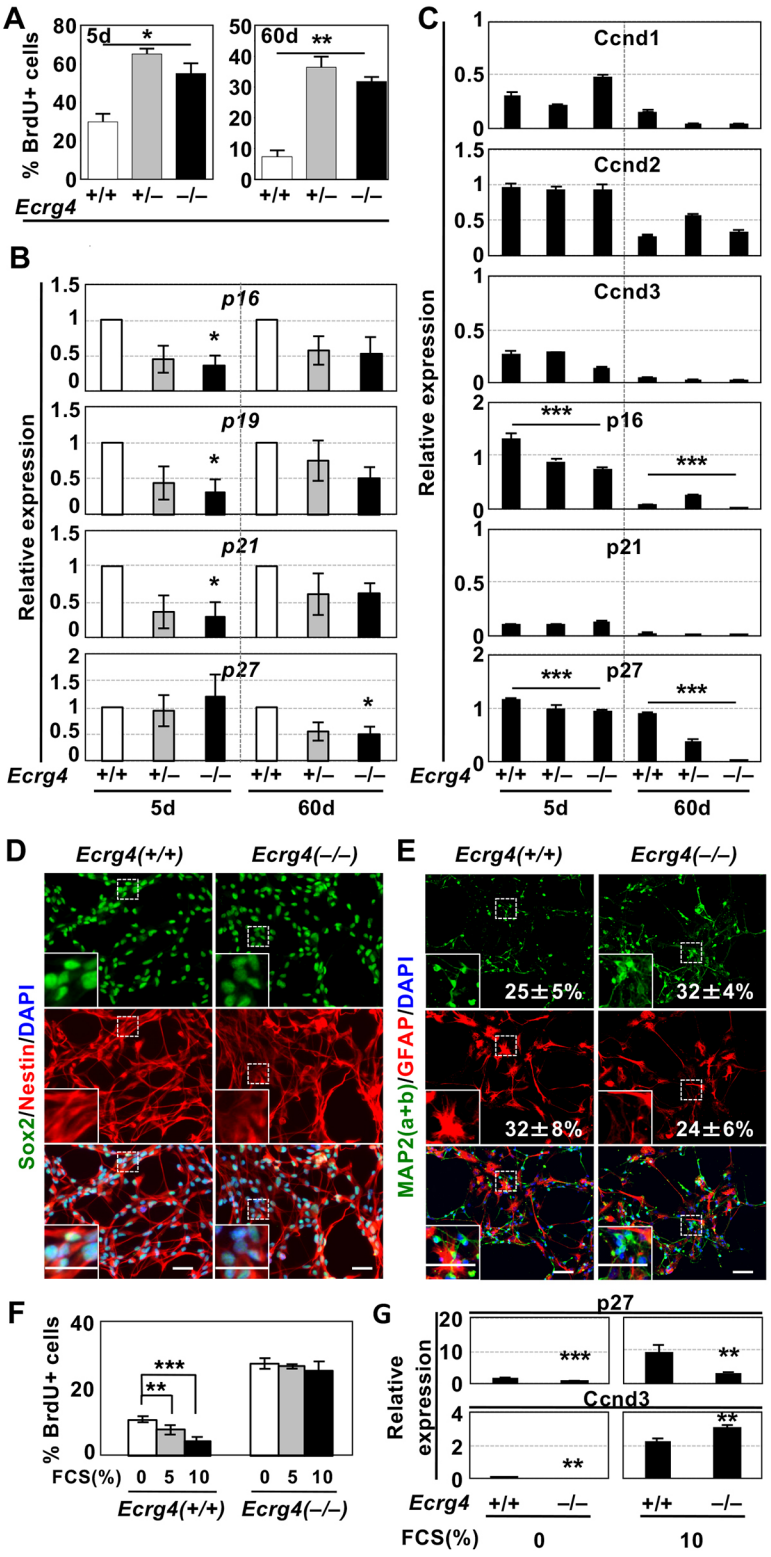

Fig. 3. Increased cell proliferation activity of *Ecrg4*$^{-/-}$ cells. (A) The proliferation of *Ecrg4*$^{+/+}$, *Ecrg4*$^{+/-}$ and *Ecrg4*$^{-/-}$ cells was measured using a BrdU incorporation assay after 5 days and 60 days in culture. Data are mean±s.e.m. of three independent experiments. (B) Quantitative RT-PCR analysis of the expression of the CDKIs *p16*, *p19*, *p21* and *p27* in the cells measured in A. The mRNA levels are shown as fold change over mRNA levels in *Ecrg4*$^{+/+}$ cells. (C) Protein levels of p16, p21, p27 and Ccnd1-Ccnd3 in the cells measured in A were shown as fold change compared with GAPDH. (D) Immunolabeling of undifferentiated *Ecrg4*$^{+/+}$ and *Ecrg4*$^{-/-}$ cells for the NSC markers (green) nestin and Sox2. (E) Immunolabeling of differentiated *Ecrg4*$^{+/+}$ and *Ecrg4*$^{-/-}$ cells for the neuronal marker MAP2(a+b) (green) and the astrocyte marker GFAP (red). Insets show the boxed regions in more detail. (F) BrdU incorporation assay of *Ecrg4*$^{+/+}$ and *Ecrg4*$^{-/-}$ cells cultured in the presence of 0% (white columns), 5% (gray columns) and 10% (black columns) FCS. (G) Protein levels of p27 and Ccnd3 in the cells shown in (F) are shown as fold change compared with GAPDH. Protein quantification was performed using ImageJ software. Data are mean±s.e.m. of three independent experiments. **P*<0.05; ***P*<0.01; ****P*<0.001. All nuclei are counterstained with DAPI (blue). Scale bars: 100 µm and 20 µm (insets) in D and E.

p27^{kip1} decreased in 60-day-old cultured Ecrg4$^{-/-}$ cells, compared with that in *Ecrg4*$^{+/+}$ cells (Jäkel et al., 2012; Nishino et al., 2008; Pagano et al., 1995; Rolfe et al., 1997) (Fig. 3B). No significant difference was observed in the expression of other CDKIs, *p15*^{ink4b} (*Cdkn2b*), *p18*^{ink4c} (*Cdkn2c*) and *p57*^{kip2} (*Cdkn1c*) between the three NSC lines (Fig. S8). Western blotting analysis confirmed the decreased expression of p16^{ink4a} and p27^{kip1} in 5- and 60-day-old cultured *Ecrg4*$^{-/-}$ cells, respectively (Fig. 3C and Fig. S9A). We also analyzed the expression of cyclin D1-D3 (Ccnd1-Ccnd3) and found that they were similarly expressed in the three NSC lines and decreased during the culture (Fig. 3C and Fig. S9A)

All of the 60-day-old cultured NSCs were positive for the definitive NSC markers nestin and Sox2, in NSC medium with the mitogens bFGF and EGF (Fig. 3D, not shown about Ecrg4$^{+/-}$). In differentiation medium, these NSCs became positive for the neuronal marker microtubule-associated protein 2 (MAP2) (a+b)

Development (2019) 146, dev168120. doi:10.1242/dev.168120

(25 and 32% in *Ecrg4*$^{+/+}$ and *Ecrg4*$^{-/-}$ cells, respectively) and astrocyte marker GFAP (32% and 24% in *Ecrg4*$^{+/+}$ and *Ecrg4*$^{-/-}$ cells, respectively) (Fig. 3E). In DMEM+10% FCS, all cells were positive for GFAP. Unexpectedly, we found that *Ecrg4*$^{-/-}$ cells continued to proliferate in this culture condition, although *Ecrg4*$^{+/+}$ cells stopped proliferating (Fig. 3F). Western blotting analysis revealed that p27^{kip1} remained low in *Ecrg4*$^{-/-}$ cells cultured in DMEM+10% FCS, whereas Ccnd3 levels slightly increased compared with those in Ecrg4$^{+/+}$ cells (Fig. 3G and Fig. S9B). The expression of other cyclin D proteins was not detected in *Ecrg4*$^{+/+}$ or *Ecrg4*$^{-/-}$ NSCs (data not shown). These data suggest that Ecrg4 deficiency drives NSC proliferation by regulating the expression of p27^{kip1}, although it was not involved in either the expression of NSC markers or in differentiation.

Foxg1 is essential for *Ecrg4*$^{-/-}$ proliferation

To further analyze how Ecrg4 deficiency enhances NSC proliferation, we compared gene expression profiles between *Ecrg4*$^{+/+}$, *Ecrg4*$^{+/-}$ and *Ecrg4*$^{-/-}$ cells and selected the increased 21 genes and decreased 19 genes (log2 ratio >2 times and <−2 times, respectively) (Fig. S10). Using quantitative RT-PCR, we confirmed decreases in the expression levels of iroquois homeobox 1 (*Irx1*) as well as *Ecrg4*, and increases in the expression levels of forkhead box g1 (*Foxg1*), six homeobox 1 (*Six1*) and DNA damage inducible transcript 4 like (*Ddit4l*) in *Ecrg4*$^{-/-}$ cells (Fig. 4A, Fig. S10B,C). Of these, we focused on Foxg1 for the following reasons: Allen Brain Atlas analysis has shown that *Foxg1* is expressed in the VZ/SVZ and DG. Furthermore, the knockout of *Foxg1* reduces NSC proliferation and induces premature neuronal differentiation (Genin et al., 2014; Tian et al., 2012; Xuan et al., 1995). Foxg1 has also been shown to prevent p21^{cip1}-dependent cell-cycle arrest and to target the *p27*^{kip1} gene (Kumamoto et al., 2013; Siegenthaler et al., 2008; Yip et al., 2012). Immunolabeling confirmed the increased expression of Foxg1 in *Ecrg4*$^{-/-}$ cells in the culture (Fig. 4B). Moreover, immunohistochemical analysis revealed that the Foxg1^{+} cell layer in the VZ/SVZ of 15 m *Ecrg4KI* mice was thicker than that of wild-type mice (Fig. 4C). These indicated that Ecrg4 negatively regulates *Foxg1* expression in NSCs *in vitro* and *in vivo*.

We next investigated whether Foxg1 regulates NSC proliferation using *Foxg1* and its specific shRNA, *foxg1sh*, expression vectors.

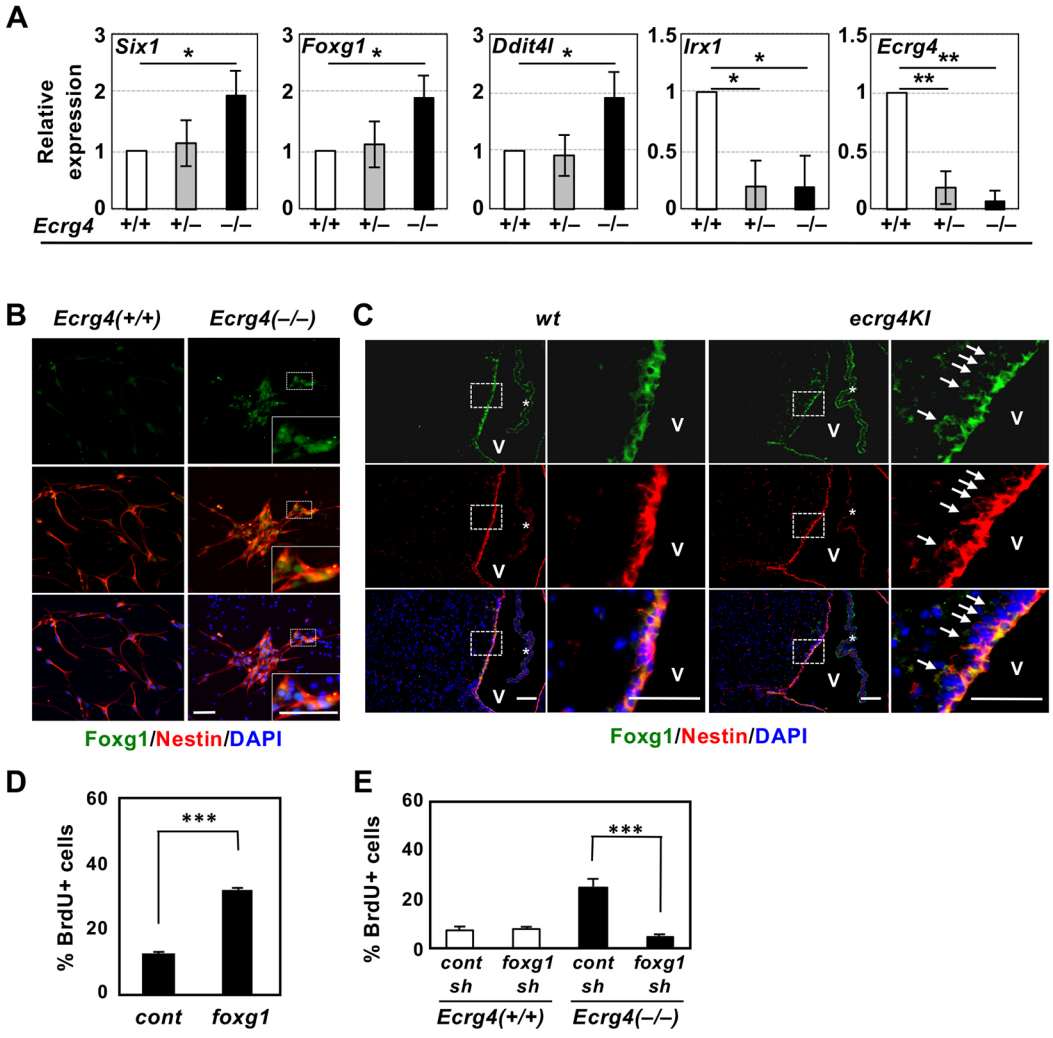

Fig. 4. Foxg1 regulates NSC proliferation as an Ecrg4 downstream factor. (A) Quantitative RT-PCR analysis of the expression of candidate genes. The mRNA levels are shown as fold change over mRNA levels in *Ecrg4*$^{+/+}$ cells. (B) Immunolabeling of *Ecrg4*$^{+/+}$ and *Ecrg4*$^{-/-}$ cells for Foxg1 (green) and nestin (red). (C) Immunolabeling of brain sections of wild type and *Ecrg4KI* for Foxg1 (green) and nestin (red). V, lateral ventricle. Stars show the choroid plexus. Nuclei are stained with DAPI (blue). (D) BrdU incorporation assay of *Ecrg4*$^{+/+}$ cells, which were transfected with a control (cont) or *Foxg1* (foxg1) expression vector in NSC medium. (E) BrdU incorporation assay of *Ecrg4*$^{+/+}$ and *Ecrg4*$^{-/-}$ cells transfected with a control shRNA (*contsh*) or *Foxg1* shRNA (*foxg1sh*) expression vector. The proportion of BrdU-positive cells is shown as the mean±s.e.m. of three cultures. **P*<0.05; ***P*<0.01; ****P*<0.001. Scale bars: 100 µm in B; 200 µm in C.

Development (2019) 146, dev168120. doi:10.1242/dev.168120

As shown in Fig. 4D, the overexpression of *Foxg1* increased the proliferation of $Ecrg4^{+/+}$ cells in culture. In contrast, the knockdown of *Foxg1* prevented the proliferation of $Ecrg4^{-/-}$ cells, whereas *foxg1sh* did not influence $Ecrg4^{+/+}$ cell proliferation (Fig. 4E). Taken together, these results demonstrated that Ecrg4 governs NSC proliferation by regulating Foxg1 expression.

Ecrg4 deficiency enhanced spatial learning and memory in mice

Age-dependent memory decline is thought to be caused by the proliferation defect and malfunction of NSCs in hippocampus (Ren et al., 2009). As $Ecrg4^{-/-}$ cells extended proliferation in the *Ecrg4KI* hippocampus (Fig. 2C), we investigated whether spatial learning and memory were better in *Ecrg4KI* mice than in wild-type mice using the Morris water maze system. As shown in Fig. 5A, wild-type and *Ecrg4KI* mice both swam at similar speeds (18.07 and 19.69 cm/s, respectively) in all experiments. On day 1, wild-type and *Ecrg4KI* mice arrived at the platform in the pool after similar times (49.6 s and 52.5 s, respectively; Movies 1 and 2). However, *Ecrg4KI* mice arrived faster than wild-type mice on day 2 (wild type versus KO, 45.5 s versus 29.3 s), and this improved further on day 3 (wild type versus KO, 41.7 versus 18.9 s; Movies 3 and 4), whereas the arrival time of wild-type mice became gradually shorter during the session although the difference was not drastic (Fig. 5B). Thus, these findings revealed that Ecrg4 deficiency enhances spatial learning and memory in mice by maintaining NSC proliferation.

DISCUSSION

One of the unanswered crucial questions for humans is how we age. Tissue-specific stem cells are undoubtedly involved in the aging process; tissue-specific stem cells continue to self-renew and supply functionally differentiated cells in their residing tissues; however, the cells gradually lose their abilities with age and eventually become senescent (Fuchs and Chen, 2013; Krieger and Simons, 2015; Liu and Rando, 2011). It is therefore crucial to find the factors that induce stem cell senescence and to characterize in order to elucidate the molecular mechanism of the aging process. Ecrg4 may fulfill the requirements of a stem cell aging factor; its expression increases in NSCs and ependymal cells with age (Kujuro et al., 2010; this study). Its overexpression induces cell senescence in NSCs and OPCs, whereas its deficiency maintains NSC proliferation *in vitro* and *in vivo* (Kujuro et al., 2010; this study). Proliferation of $Ecrg4^{-/-}$ cells significantly decreased when cultured with $Ecrg4^{+/+}$ cells (this study). Ecrg4 has been shown to induce the expression of pro-inflammatory factors, which are involved in the initiation and maintenance of cell senescence in microglia/macrophages through the activation of scavenger receptor/NF-κB signaling pathway (Kizil et al., 2015; Moriguchi et al., 2016, 2018). Furthermore, we have demonstrated here that Ecrg4 deficiency increased spatial learning and memory in mice. Collectively, these findings suggest that Ecrg4 induces NSCs to be senescent in an autocrine/paracrine manner or through the activation of their surrounding cells, such as microglia/macrophage. Therefore, the inhibition of Ecrg4 may maintain brain function at high levels, even in the aged brain.

We detected *Ecrg4* promoter activity in the ependymal layer and VZ/SVZ using *Ecrg4KI* mice, suggesting that NSC- and ependymal cell-specific transcription factors/regulators induce the expression of *Ecrg4*. This hypothesis is supported by the Champion ChiP Transcription Factor Search Portal (Qiagen) showing that the Ecrg4 promoter contains potential binding sites for Sox, Myb and Foxj1, which are essential for NSC maintenance and ependymal cell differentiation (Johe et al., 1996; Kyrousi et al., 2015; Stubbs et al., 2008; Zappone et al., 2000). *Let7b* and its targets, HMGA2 and Igf2bp1, are also candidates for Ecrg4 expression, because they are not only expressed in VZ/SVZ and DG but have also been shown to play roles in NSC aging (Nishino et al., 2008, 2013; Yang et al., 2015). Elucidation of the molecular mechanisms by which the expression of Ecrg4 is induced in NSCs and ependymal cells would provide an important insight involved in the initiation of NSC aging.

We found the differences in the expression of $p16^{ink4a}$ and $p27^{kip1}$ between $Ecrg4^{-/-}$ and $Ecrg4^{+/+}$ cells. $p27^{kip1}$ was shown to be negatively regulated by Src-, JAK2- and Lyn-dependent phosphorylation and the proteasome pathway (Grimmler et al., 2007). As our microarray analysis revealed an increase in the expression of *Lyn* in $Ecrg4^{-/-}$ cells, Lyn may induce $p27^{kip1}$ degradation in $Ecrg4^{-/-}$ cells. Foxg1 is another candidate factor that decreases $p27^{kip1}$ expression, as it was shown that Foxg1 directly targeted $p27^{kip1}$ gene (Kumamoto et al., 2013; this study). Much evidence has demonstrated the transcriptional and post-transcriptional regulation of $p16^{ink4a}$ by inhibitor of differentiation 1, polycomb group complexes, microRNA-24, etc. (LaPak and Burd, 2014). As the expression of these candidate factors did not change between $Ecrg4^{-/-}$ and $Ecrg4^{+/+}$ cells in our microarray data, it remains unknown which factor induces the accumulation of $p16^{ink4a}$ in NSCs.

It was surprising that $Ecrg4^{+/-}$ cells showed an increase in proliferation in the same way that $Ecrg4^{-/-}$ cells did, although *Foxg1* levels did not increase in $Ecrg4^{+/-}$ cells, suggesting that an unknown Ecrg4-downstream factor/mechanism, other than Foxg1, is also involved in cell proliferation. One possible mechanism is that the combination of the increased level of Ccnd2 with the decreased expression of $p15^{ink4b}$ and $p57^{kip2}$, compared with $Ecrg4^{-/-}$ cells, might enhance $Ecrg4^{+/-}$ cell proliferation (Fig. 3C and Fig. S8). The expression of these cell-cycle regulators may be controlled by the crosstalk of Ecrg4 receptor signaling pathways, as Ecrg4 binds multiple scavenger receptors (Moriguchi et al., 2018). It is, therefore, essential in future to understand whole signaling pathways that Ecrg4 regulates.

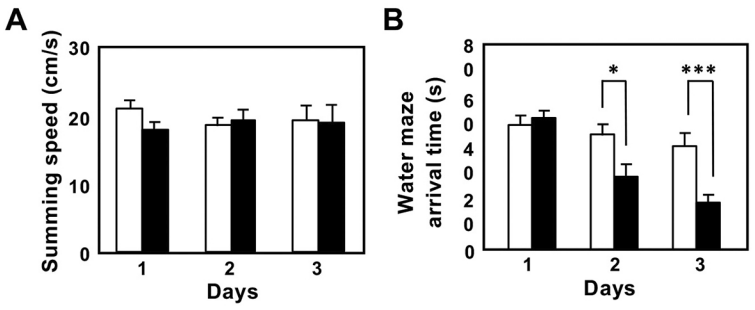

Fig. 5. The Morris water maze test reveals increases in spatial learning and memory in *Ecrg4KI* mice. (A,B) Summing speed (A) and arrival time (B) of wild-type (white column) and *Ecrg4KI* (black column) mice in the Morris water maze paradigm on days 1-3. Data are mean±s.e.m. of three independent experiments (n=6 mice). *P<0.05; ***P<0.001.

Development (2019) 146, dev168120. doi:10.1242/dev.168120

Microarray analyses identified Foxg1 that is negatively regulated by Ecrg4 signaling. Because Ecrg4 has been shown to activate the NF-κB signaling pathway by binding with its receptors (Moriguchi et al., 2018), we searched the putative NF-κB binding sites in mouse *Foxg1* promoter region using the transcription factor binding sites search engine PROMO (alggen.lsi.upc.es/cgi-bin/promo_v3/promo/promoinit.cgi?dirDB=TF_8.3) and found one NF-κB target site. Although there is much evidence that NF-κB acts as a transcription activator, it may repress *Foxg1* expression with epigenetic modifiers, including enhancer of zeste homolog 2 (EZH2), binding sites for which also exist in the *Foxg1* promoter.

Water maze analysis revealed that Ecrg4 deficiency increased the spatial learning and memory in mice. As Ecrg4 induces the expression of pro-inflammatory factors in microglia/macrophage, inhibition of Ecrg4-dependent inflammatory pathway may make it possible to maintain brain function better. Similarly, it is of great interest to study whether Ecrg4-dependent chronic inflammation causes a functional decline in various types of tissues.

MATERIALS AND METHODS

Animals and chemicals

Mice were obtained from Charles River Japan. *Ecrg4KI* mice (accession number CDB0712K; www2.clst.riken.jp/arg/mutant%20mice%20list.html) were generated using a knock-in method described previously (www2.clst.riken.jp/arg/methods.html) (Fig. S1A). *Ecrg4KI* mice were crossed with ACTB-FLPe mice (Rodríguez et al., 2000) to delete the neomycin selection cassette, generating $Ecrg4^{floxed\text{-}lacZ/+}$ mice, and were backcrossed and maintained on a C57BL/6 genetic background. The genotype of each mouse was confirmed by a Southern blot analysis and PCR (Fig. S1B and S1C). All mouse experimental protocols were approved by the Animal Care and Use Committees of RIKEN Kobe Branch and Hokkaido University. Chemicals and growth factors were purchased from Sigma-Aldrich and PeproTech, respectively, except where otherwise indicated.

Preparation of the VZ/SVZ and hippocampus cells

The VZ/SVZ and hippocampus were dissected from 6-month-old *Ecrg4hetero* mice under a Stemi 2000 microscope (Carl Zeiss). The collected tissues were cut as small as possible and the cells were dispersed using the Papain dissociation system (Worthington).

Cell culture

Mouse primary NSCs were cultured as floating spheres in DMEM/F12 (Gibco) supplemented with the chemicals bFGF (10 ng/ml) and EGF (10 ng/ml) (NSC medium) in a standard culture dish (Falcon) for up to 60 days, as described previously (Kondo and Raff, 2000, 2004). For immunolabeling, cells were cultured as a monolayer on poly-D-lysine (PDL, 15 µg/ml) and fibronectin (1 µg/ml, Invitrogen)-coated dishes in NSC medium. In order to induce neural differentiation, NSCs were cultured on PDL- and fibronectin-coated eight-well chamber slides (Nunc) in mitogen-free NSC medium with 0.5% FCS (differentiation medium) or DMEM +10% FCS for 1 week. A BrdU incorporation assay was performed to quantify cell proliferation, as described previously (Kondo and Raff, 2004).

Immunochemistry

Immunostaining of brain sections (6-10 µm) was performed as described previously (Kujuro et al., 2010; Nishide et al., 2009). Sections were permeabilized with 0.3% Triton X-100 in PBS for penetration, treated with a blocking solution (2% skim milk, 0.3% Triton X-100 and PBS) for 1 h, and incubated with primary antibodies for 16 h at 4°C. Cells were fixed and immunostained as described previously (Hide et al., 2009; Kondo and Raff, 2000, 2004; Nishide et al., 2009). The following antibodies were used to detect antigens: mouse monoclonal anti-nestin (1:200, BD, Rat401), rabbit polyclonal anti-GFAP (1:500, DakoCytomation, Z0334), mouse monoclonal anti-GFAP (Sigma; 1:400, G3893), chicken anti-β-gal (1:500, Abcam, ab9361), rabbit polyclonal anti-Sox2 (1:500, StemCell Technology, 01438), mouse monoclonal anti-MAP2(a+b) (1:200, Abcam, ab5392), rabbit monoclonal anti-Ki67 (1:100, Thermo Fisher Scientific, Clone SP6), rabbit polyclonal anti-Foxg1 (1:100, Novus Biologicals, NBP1-56594), mouse monoclonal anti-PSA-NCAM (1:500, 12E3, a kind gift from Dr Tatsunori Seki, Tokyo Medical University, Japan), rabbit polyclonal anti-Ecrg4 (1:100, Sigma, HPA008546), rabbit anti-Histone H3 phospho serine10 (1:200, Abcam, ab47297) and anti-BrdU (1:100, DSHB, G3G4). Antibodies were detected using Alexa568-conjugated goat anti-rabbit (1:500, Thermo Fisher Scientific, A-11036), Alexa568-conjugated goat anti-mouse (1:500, Thermo Fisher Scientific, A-11004), Alexa488-conjugated goat anti-rabbit (1:500, Thermo Fisher Scientific, A-11008), Alexa488-conjugated goat anti-mouse (1:500, Thermo Fisher Scientific, R37120) and Cy3-conjugated donkey anti-chicken (1:500, Jackson ImmunoResearch, 703-165-155). Cells were counterstained with DAPI (1 µg/ml, DOJINDO, D523) to visualize nuclei. Fluorescence images were obtained using an AxioImager M1 microscope (Carl Zeiss).

Flow cytometry analysis

The VZ/SVZ cells were treated with the SPiDER-βGal reagent for β-gal activity, according to the supplier's instructions (Dojin), and then analyzed in an Aria II (Becton Dickinson) using a dual-wavelength analysis (488 nm solid-state laser and 638 nm semiconductor laser). Propidium iodide (PI)-positive (i.e. dead) cells were excluded from the analysis.

Brain fixation and histochemistry

Dissected mouse brains were fixed in 4% paraformaldehyde at 4°C overnight. After fixation, the brains were cryoprotected with 12-18% sucrose in PBS and embedded in Tissue-Tek OCT compound (Miles). In X-gal staining, frozen 10 µm sagittal sections were fixed using 0.2% glutaraldehyde in PBS for 5 min, washed several times and stained using an X-gal staining solution (2 mg/ml X-gal) for 24 h, as described previously (Nishide et al., 2009). For immunohistochemical analyses, the antigens were retrieved by HistoVT One, according to the supplier's instructions (Nacalai Tesque). X-gal staining images were obtained using a BZ-X800 microscope (Keyence).

Quantitative RT-PCR

Real-time PCR was performed on the StepOnePlus (Thermo Fisher Scientific) using THUNDERBIRD SYBR qPCR Mix (TOYOBO), according to the manufacturer's protocol. Cycle parameters were 15 s at 95°C and 30 s at 60°C for 40 cycles. All gene expression data were normalized to the housekeeping gene 18S ribosomal RNA, according to the ΔΔCt method. The sequences of the oligonucleotide primers are shown in Table S1.

Vector construction

Complementary DNAs (cDNAs) were cloned as described previously (Kondo and Raff, 2000, 2004). Mouse *Foxg1* cDNA was inserted into the pMX-EGFP vector to produce pMX-EGFP-mfoxg1. The following oligonucleotide DNA primers were synthesized to amplify full mouse *Foxg1* cDNA: 5′ primer, 5′-AGAATTCGCCACCATGCTGGACATGG-GAGATAGG-3′; 3′ primer, 5′-ACTCGAGTTAATGTATTAAAGGGTT-GGAAGAAGA-3′.

In order to knockdown mouse *Foxg1*, short-hairpin (sh) sequences were generated using InvivoGen's siRNA Wizard (www.sirnawizard.com/). These sh sequences were inserted into a psiRNA-h7SKhygro G1 expression vector (InvivoGen) to produce psiRNA-h7SKhygro-mfoxg1sh. The knockdown efficiency of the vector was analyzed by western blotting (Fig. S11). The sh target sequence for mouse *foxg1* was 5′-GTCTTCTT-CCAACCCTTTAAT-3′. The control sh target (*egfp*) sequence was 5′-G-CAAGCTGACCCTGAAGTTCA-3′. The nucleotide sequences of cloned cDNA and inserted shRNA were verified using the BigDye Terminator Kit version 3.1 (Applied Biosystems) and ABI sequencer model 3130xl (Applied Biosystems). We transfected the cells with vectors using either the Nucleofector device according to the supplier's instructions (Lonza) or Polyethylenimine (PEI), as previously described (Kondo and Raff, 2004; Nishide et al., 2009).

Gene microarray analysis

Total RNA was prepared from the cultured NSCs and the dissociated VZ/SVZ cells, and then used for microarray analysis with the 3D-Gene Mouse Oligo chip 24k (TORAY) and the mouse GE 8×60K microarray (Agilent), as previously described (Kaneko et al., 2015; Ohtsu et al., 2016). Microarray data have been deposited in GEO under accession numbers GSE120626 and GSE120749.

Western blotting

Western blotting was performed as previously described (Takanaga et al., 2009). The blotted membranes were probed for the following antigens: $p16^{Ink4a}$ (Santa Cruz, 1:200), $p21^{Cip1}$ (Santa Cruz, 1:100), $p27^{Kip1}$ (Cell Signaling Technology, 1:500), Ccnd1 (Cell Signaling Technology, 1:500), Ccnd2 (Abcam, 1:100), Ccnd3 (Cell Signaling Technology, 1:2000) and GAPDH (Chemicon, 1:1000). An ECL system (Amersham) was used for detection. Protein quantification was performed using ImageJ software (NIH).

Morris water maze test

The Morris water maze test for the cognitive functional examination was performed in the New Drug Research Center (Sapporo, Japan) as previously described (Taniguchi et al., 2005). In brief, mice were tested in a maze that was 90 cm in diameter (LE82090, Nihon Bioresearch) containing water at 22°C with a round platform (diameter of 11 cm), which was submerged 0.5 cm beneath the water surface. The test was performed after 3 days of acquisition training with three trials per day. Mice (approximately 6 months old) were released at one of three randomly varied points and were given 60 s to find the platform. If the mice failed to find the platform within the time allotted, they were manually placed on the platform for 10 s and latency was recorded as 60 s. Mice were videoed and tracked using a LOGICOOL HD Webcam C615. Swimming speed was analyzed by Smart V3.0 software.

Statistical analysis

All studies were analyzed using a two-tailed Student's *t*-test, with a significant difference being defined as $P<0.05$.

Acknowledgements

We thank Shuji Takeda and Uichi Koshimizu for their helpful comments and critical reading of the manuscript; Tatsunori Seki for mouse anti-PSA-NCAM monoclonal antibody, Toshihiro Hata, Sachiyo Kawami, Kanako Ohyama and Naoki Ikeda for their technical assistance; and Satoshi Kondou for performing the DNA microarray analysis.

Competing interests

The authors declare no competing or financial interests.

Author contributions

Conceptualization: T.K.; Methodology: Y.N., H.K., T.K.; Validation: Y.N., T.K.; Formal analysis: Y.N., H.K., T.K.; Investigation: Y.N., H.K., T.K.; Resources: Y.N., H.K., T.K.; Data curation: Y.N., H.K., T.K.; Writing - original draft: T.K.; Visualization: Y.N., T.K.; Supervision: T.K.; Project administration: T.K.; Funding acquisition: T.K.

Funding

This work was partly supported by a RIKEN internal grant (to T.K.), a research grant from Asubio Pharma Corporation (to T.K.) and was carried out under the Joint Research Program of the Institute for Genetic Medicine, Hokkaido University (to T.K.).

Data availability

Microarray data have been deposited in GEO under accession numbers GSE120626 and GSE120749.

Supplementary information

Supplementary information available online at
http://dev.biologists.org/lookup/doi/10.1242/dev.168120.supplemental

References

Doetsch, F., Caillé, I., Lim, D. A., García-Verdugo, J. M. and Alvarez-Buylla, A. (1999). Subventricular zone astrocytes are neural stem cells in the adult mammalian brain. *Cell* **97**, 703-716.

Farkas, L. M. and Huttner, W. B. (2008). The cell biology of neural stem and progenitor cells and its significance for their proliferation versus differentiation during mammalian brain development. *Curr. Opin. Cell Biol.* **20**, 707-715.

Fuchs, E. and Chen, T. (2013). A matter of life and death: self-renewal in stem cells. *EMBO Rep.* **14**, 39-48.

Genin, E. C., Caron, N., Vandenbosch, R., Nguyen, L. and Malgrange, B. (2014). Forkhead pathway in the control of adult neurogenesis. *Stem Cells* **32**, 1398-1407.

Gonzalez, A. M., Podvin, S., Lin, S.-Y., Miller, M. C., Botfield, H., Leadbeater, W. E., Roberton, A., Dang, X., Knowling, S. E., Cardenas-Galindo, E. et al. (2011). Ecrg4 expression and its product augurin in the choroid plexus: impact on fetal brain development, cerebrospinal fluid homeostasis and neuroprogenitor cell response to CNS injury. *Fluids Barriers CNS* **8**, 6.

Goodell, M. A., Nguyen, H. and Shroyer, N. (2015). Somatic stem cell heterogeneity: diversity in the blood, skin and intestinal stem cell compartments. *Nat. Rev. Mol. Cell Biol.* **16**, 299-309.

Götze, S., Feldhaus, V., Traska, T., Wolter, M., Reifenberger, G., Tannapfel, A., Kuhnen, C., Martin, D., Müller, O. and Sievers, S. (2009). ECRG4 is a candidate tumor suppressor gene frequently hypermethylated in colorectal carcinoma and glioma. *BMC Cancer* **9**, 447.

Grimmler, M., Wang, Y., Mund, T., Cilenšek, Z., Keidel, E.-M., Waddell, M. B., Jäkel, H., Kullmann, M., Kriwacki, R. W. and Hengst, L. (2007). Cdk-inhibitory activity and stability of p27Kip1 are directly regulated by oncogenic tyrosine kinases. *Cell* **128**, 269-280.

Hide, T., Takezaki, T., Nakatani, Y., Nakamura, H., Kuratsu, J. and Kondo, T. (2009). Sox11 prevents tumorigenesis of glioma-initiating cells by inducing neuronal differentiation. *Cancer Res.* **69**, 7953-7959.

Jäkel, H., Peschel, I., Kunze, C., Weinl, C. and Hengst, L. (2012). Regulation of p27 (Kip1) by mitogen-induced tyrosine phosphorylation. *Cell Cycle* **11**, 1910-1917.

Johe, K. K., Hazel, T. G., Muller, T., Dugich-Djordjevic, M. M. and McKay, R. D. (1996). Single factors direct the differentiation of stem cells from the fetal and adult central nervous system. *Genes Dev.* **10**, 3129-4310.

Kaneko, S., Nakatani, Y., Takezaki, T., Hide, T., Yamashita, D., Ohtsu, N., Ohnishi, T., Terasaka, S., Houkin, K. and Kondo, T. (2015). Ceacam1L modulates STAT3 signaling to control the proliferation of glioblastoma-initiating cells. *Cancer Res.* **75**, 4224-4234.

Kizil, C., Kyritsis, N. and Brand, M. (2015). Effects of inflammation on stem cells: together they strive? *EMBO Rep.* **16**, 416-426.

Kondo, T. and Raff, M. (2000). Oligodendrocyte precursor cells reprogrammed to become multipotential CNS stem cells. *Science* **289**, 1754-1757.

Kondo, T. and Raff, M. (2004). Chromatin remodeling and histone modification in the conversion of oligodendrocyte precursors to neural stem cells. *Genes Dev.* **18**, 2963-2972.

Krieger, T. and Simons, B. D. (2015). Dynamic stem cell heterogeneity. *Development* **142**, 1396-1406.

Kujuro, Y., Suzuki, N. and Kondo, T. (2010). Esophageal cancer-related gene 4 is secreted inducer of cell senescence expressed by aged CNS precursor cells. *Proc. Natl. Acad. Sci. USA* **107**, 8259-8264.

Kumamoto, T., Toma, K., Gunadi, K., McKenna, W. L., Kasukawa, T., Katzman, S., Chen, B. and Hanashima, C. (2013). Foxg1 coordinates the switch from nonradially to radially migrating glutamatergic subtypes in the neocortex through spatiotemporal repression. *Cell Rep.* **3**, 931-945.

Kyrousi, C., Arbi, M., Pilz, G.-A., Pefani, D.-E., Lalioti, M.-E., Ninkovic, J., Götz, M., Lygerou, Z. and Taraviras, S. (2015). Mcidas and GemC1 are key regulators for the generation of multiciliated ependymal cells in the adult neurogenic niche. *Development* **142**, 3661-3674.

LaPak, K. M. and Burd, C. E. (2014). The molecular balancing act of p16(INK4a) in cancer and aging. *Mol. Cancer Res.* **12**, 167-183.

Lee, J., Dang, X., Borboa, A., Coimbra, R., Baird, A. and Eliceiri, B. P. (2015). Thrombin-processed Ecrg4 recruits myeloid cells and induces antitumorigenic inflammation. *Neuro. Oncol.* **17**, 685-696.

Li, L.-W., Yu, X.-Y., Yang, Y., Zhang, C.-P., Guo, L.-P. and Lu, S.-H. (2009). Expression of esophageal cancer related gene 4 (ECRG4), a novel tumor suppressor gene, in esophageal cancer and its inhibitory effect on the tumor growth in vitro and in vivo. *Int. J. Cancer* **125**, 1505-1513.

Li, W., Liu, X., Zhang, B., Qi, D., Zhang, L., Jin, Y. and Yang, H. (2010). Overexpression of candidate tumor suppressor ECRG4 inhibits glioma proliferation and invasion. *J. Exp. Clin. Cancer Res.* **29**, 89.

Liu, L. and Rando, T. A. (2011). Manifestations and mechanisms of stem cell aging. *J. Cell Biol.* **193**, 257-266.

Moriguchi, T., Kaneumi, S., Takeda, S., Enomoto, K., Mishra, S. K., Miki, T., Koshimizu, U., Kitamura, H. and Kondo, T. (2016). Ecrg4 contributes to the anti-glioma immunosurveillance through type I interferon signalling. *OncoImmunology* **5**, e1242547.

Moriguchi, T., Takeda, S., Iwashita, S., Enomoto, K., Koshimizu, U. and Kondo, T. (2018). Ecrg4 peptide is the ligand of multiple scavenger receptors. *Sci. Rep.* **8**, 4048.

Nishide, K., Nakatani, Y., Kiyonari, H. and Kondo, T. (2009). Glioblastoma formation from cell population depleted of Prominin1-expressing cells. *PLoS ONE* **4**, e6869.

Nishino, J., Kim, I., Chada, K. and Morrison, S. J. (2008). Hmga2 promotes neural stem cell self-renewal in young but not old mice by reducing p16Ink4a and p19Arf Expression. *Cell* **135**, 227-239.
Nishino, J., Kim, S., Zhu, Y., Zhu, H. and Morrison, S. J. (2013). A network of heterochronic genes including Imp1 regulates temporal changes in stem cell properties. *eLife* **2**, e00924.
Ohtsu, N., Nakatani, Y., Yamashita, D., Ohue, S., Ohnishi, T. and Kondo, T. (2016). Eva1 maintains the stem-like character of glioblastoma-initiating cells by activating the non-canonical NF-κB signaling pathway. *Cancer Res.* **76**, 171-181.
Pagano, M., Tam, S. W., Theodoras, A. M., Beer-Romero, P., Del Sal, G., Chau, V., Yew, P. R., Draetta, G. F. and Rolfe, M. (1995). Role of the ubiquitin-proteasome pathway in regulating abundance of the cyclin-dependent kinase inhibitor p27. *Science* **269**, 682-685.
Ren, J.-L., Pan, J.-S., Lu, Y.-P., Sun, P. and Han, J. (2009). Inflammatory signaling and cellular senescence. *Cell. Signal.* **21**, 378-383.
Rodríguez, C. I., Buchholz, F., Galloway, J., Sequerra, R., Kasper, J., Ayala, R., Stewart, A. F. and Dymecki, S. M. (2000). High-efficiency deleter mice show that FLPe is an alternative to Cre-loxP. *Nat. Genet.* **25**, 139-140.
Rolfe, M., Chiu, M. I. and Pagano, M. (1997). The ubiquitin-mediated proteolytic pathway as a therapeutic area. *J. Mol. Med.* **75**, 5-17.
Sabatier, R., Finetti, P., Adelaide, J., Guille, A., Borg, J.-P., Chaffanet, M., Lane, L., Birnbaum, D. and Bertucci, F. (2011). Down-regulation of ECRG4, a candidate tumor suppressor gene, in human breast cancer. *PLoS ONE* **6**, e27656.
Siegenthaler, J. A., Tremper-Wells, B. A. and Miller, M. W. (2008). Foxg1 haploinsufficiency reduces the population of cortical intermediate progenitor cells: effect of increased p21 expression. *Cereb. Cortex* **18**, 1865-1875.
Steiner, J., Bernstein, H.-G., Bielau, H., Berndt, A., Brisch, R., Mawrin, C., Keilhoff, G. and Bogerts, B. (2007). Evidence for a wide extra-astrocytic distribution of S100B in human brain. *BMC Neurosci.* **8**, 2.
Stubbs, J. L., Oishi, I., Izpisúa Belmonte, J. C. and Kintner, C. (2008). The forkhead protein Foxj1 specifies node-like cilia in Xenopus and zebrafish embryos. *Nat. Genet.* **40**, 1454-1460.
Su, T., Liu, H. and Lu, S. (1998). Cloning and identification of cDNA fragments related to human esophageal cancer. *Zhonghua Zhong Liu Za Zhi* **20**, 254-257.
Takanaga, H., Tsuchida-Straten, N., Nishide, K., Watanabe, A., Aburatani, H. and Kondo, T. (2009). Gli2 is a novel regulator of Sox2 expression in telencephalic neuroepithelial cells. *Stem Cells* **27**, 165-174.
Taniguchi, T., Doe, N., Matsuyama, S., Kitamura, Y., Mori, H., Saito, N. and Tanaka, C. (2005). Transgenic mice expressing mutant (N279K) human tau show mutation dependent cognitive deficits without neurofibrillary tangle formation. *FEBS Lett.* **579**, 5704-5712.
Tian, C., Gong, Y., Yang, Y., Shen, W., Wang, K., Liu, J., Xu, B., Zhao, J. and Zhao, C. (2012). Foxg1 has an essential role in postnatal development of the dentate gyrus. *J. Neurosci.* **32**, 2931-2949.
Tramontin, A. D., García-Verdugo, J. M., Lim, D. A. and Alvarez-Buylla, A. (2003). Postnatal development of radial glia and the ventricular zone (VZ): a continuum of the neural stem cell compartment. *Cereb. Cortex* **13**, 580-587.
Xu, T., Xiao, D. and Zhang, X. (2013). ECRG4 inhibits growth and invasiveness of squamous cell carcinoma of the head and neck in vitro and in vivo. *Oncol. Lett.* **5**, 1921-1926.
Xuan, S., Baptista, C. A., Balas, G., Tao, W., Soares, V. C. and Lai, E. (1995). Winged helix transcription factor BF-1 is essential for the development of the cerebral hemispheres. *Neuron* **14**, 1141-1152.
Yang, M., Yang, S.-L., Herrlinger, S., Liang, C., Dzieciatkowska, M., Hansen, K. C., Desai, R., Nagy, A., Niswander, L., Moss, E. G. et al. (2015). Lin28 promotes the proliferative capacity of neural progenitor cells in brain development. *Development* **142**, 1616-1627.
Yip, D. J., Corcoran, C. P., Alvarez-Saavedra, M., DeMaria, A., Rennick, S., Mears, A. J., Rudnicki, M. A., Messier, C. and Picketts, D. J. (2012). Snf2l regulates Foxg1-dependent progenitor cell expansion in the developing brain. *Dev. Cell* **22**, 871-878.
Yue, C.-M., Deng, D. J., Bi, M. X., Guo, L. P. and Lu, S. H. (2003). Expression of ECRG4, a novel esophageal cancer-related gene, downregulated by CpG island hypermethylation in human esophageal squamous cell carcinoma. *World J. Gastroenterol.* **9**, 1174-1178.
Zappone, M. V., Galli, R., Catena, R., Meani, N., De Biasi, S., Mattei, E., Tiveron, C., Vescovi, A. L., Lovell-Badge, R., Ottolenghi, S. et al. (2000). Sox2 regulatory sequences direct expression of a (beta)-geo transgene to telencephalic neural stem cells and precursors of the mouse embryo, revealing regionalization of gene expression in CNS stem cells. *Development* **127**, 2367-2382.

Supplementary Information

Supplementary Figures

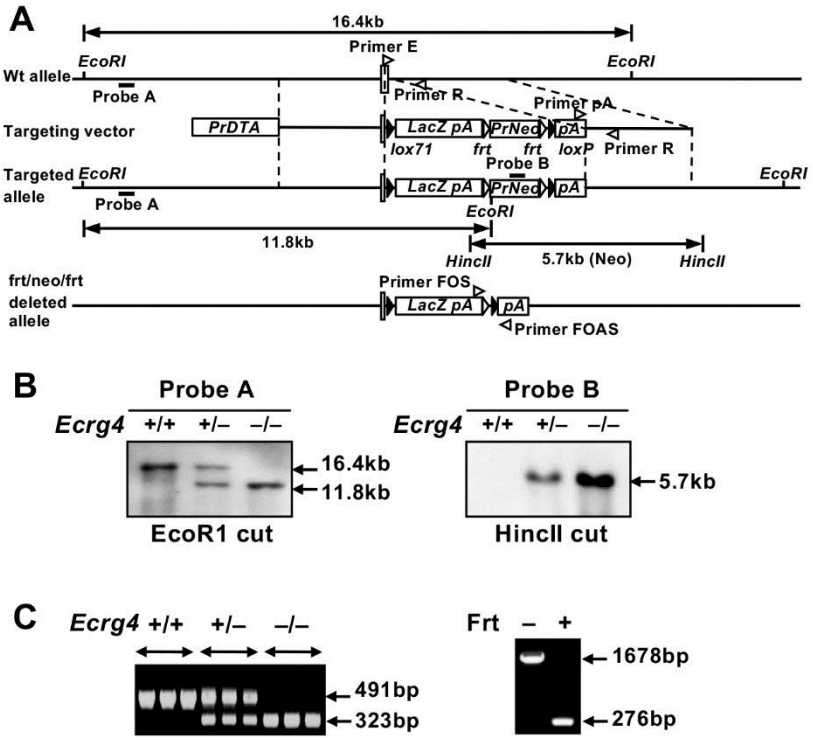

Fig. S1. Generation of *ecrg4KI* mice

(A): Schematic representation of the targeted allele. (B): A Southern blot analysis of the *ecrg4*$^{+/+}$ (+/+), *ecrg4*$^{floxed\text{-}lacZ/+}$(+/-), and *ecrg4*$^{floxed\text{-}lacZ/\ floxed\text{-}lacZ}$ (-/-) lines. (C): A genomic PCR analysis of three independent (+/+), (+/-), and (-/-) lines (left panel) and a floxed line (Frt, right panel).

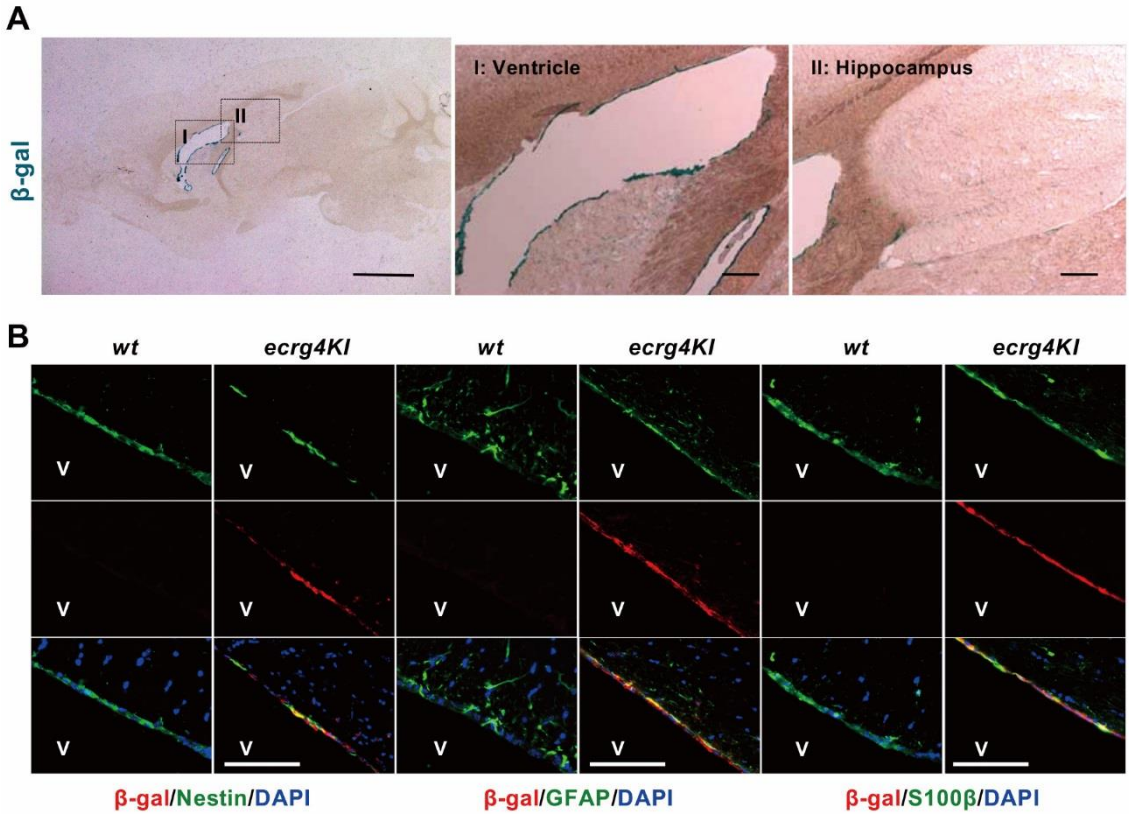

Fig. S2. Ecrg4 promoter activity in the ependymal cell layer

(A): X-gal staining (blue) of frozen brain sections of 15m *ecrg4KI*. Insets (I and II) show high magnification images of Ventricle and hippocampus, respectively. (B): Immunostaining of brain sections of 15m *wt* and *ecrg4KI* for β-gal (red) and neural markers (green), Nestin (left panels), GFAP (middle panels), and S100β (right panels). All nuclei were counterstained with DAPI (blue). V: lateral ventricle. Scale, 2 mm in A; 200 μm in B.

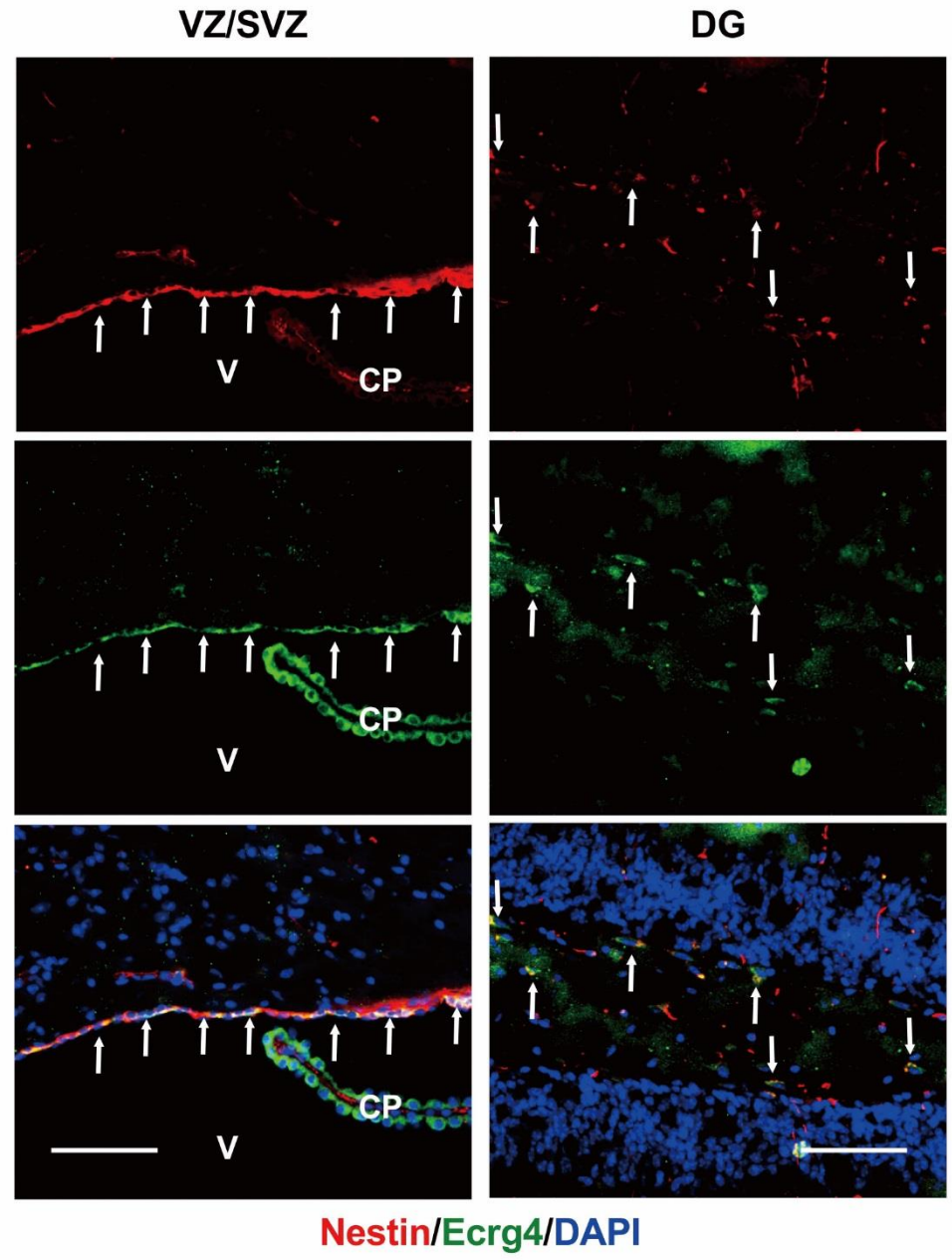

Fig. S3. Ecrg4 expression in VZ/SVZ and DG

Immunostaining of brain sections of 6m *wt* for Ecrg4 (green) and Nestin (red). All nuclei were counterstained with DAPI (blue). Arrows indicate Ecrg4 and Nestin double positive cells in VZ/SVZ and DG. V: lateral ventricle. CP: choroid plexus. Scale, 100 μ m.

A

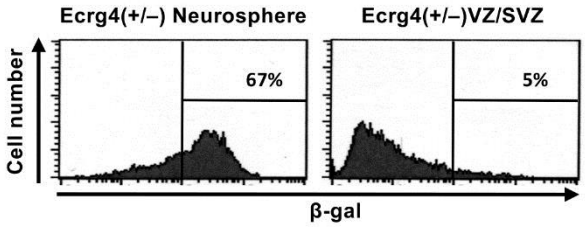

B

Gene symbol	Gene name	Fold change (VZ/SVZ vs Neurosphere)	Raw data (VZ/SVZ)	Raw data (Neurosphere)	Specificity
Foxg1	forkhead box G1	496.07	618.02	1.17	NSC
Aqp1	aquaporin 1	122.56	770.78	5.89	Ependymal
Gfap	glial fibrillary acidic protein	54.19	194.76	3.37	Ependymal
Ctgf	connective tissue growth factor	29.37	2,665.53	85.05	Ependymal
Fut4 (SSEA1, CD15)	fucosyltransferase 4	21.22	88.85	3.92	NSC
Prdm16	PR domain containing 16	19.54	73.91	3.54	NSC
Gabrg1	gamma-aminobutyric acid (GABA) A receptor, subunit gamma 1	16.25	29.15	1.68	Ependymal
Icam1	intercellular adhesion molecule 1	14.23	18.64	1.23	Ependymal
Angptl4	angiopoietin-like 4	11.44	548.85	44.97	Ependymal
Notch4	notch 4	11.27	148.87	12.37	Ependymal
Angptl1	angiopoietin-like 1	10.46	24.89	2.23	Ependymal
Angptl2	angiopoietin-like 2	10.42	111.84	10.06	Ependymal
Aqp4	aquaporin 4	8.16	42.98	4.94	Ependymal
Gabrg3	gamma-aminobutyric acid (GABA) A receptor, subunit gamma 3	7.52	8.90	1.11	Ependymal
Aqp6	aquaporin 6	7.16	38.85	5.08	Ependymal
Cxcr4	chemokine (C-X-C motif) receptor 4	6.90	1,627.70	220.95	Ependymal
Dlx2	distal-less homeobox 2	6.67	110.38	15.51	Ependymal
Vegfa	vascular endothelial growth factor A	6.37	1,948.54	286.66	Ependymal
Gabra3	gamma-aminobutyric acid (GABA) A receptor, subunit alpha 3	6.24	7.89	1.18	Ependymal
Rfx3	regulatory factor X, 3 (influences HLA class II expression)	5.96	6.58	1.03	Ependymal
Icam2	intercellular adhesion molecule 2	5.32	44.44	7.83	Ependymal
Icam4	intercellular adhesion molecule 4, Landsteiner-Wiener blood group	4.21	8.89	1.98	Ependymal
Id2	inhibitor of DNA binding 2	3.79	236.19	58.33	Ependymal
Gabrb2	gamma-aminobutyric acid (GABA) A receptor, subunit beta 2	3.66	43.09	11.04	Ependymal
Gabarap	gamma-aminobutyric acid receptor associated protein	3.61	89.02	23.14	Ependymal
Aqp3	aquaporin 3	3.00	30.37	9.49	Ependymal
Aqp5	aquaporin 5	2.78	25.04	8.43	Ependymal
Ptprc (CD45)	protein tyrosine phosphatase, receptor type, C	2.48	20.55	7.76	Ependymal
Hgf	hepatocyte growth factor	2.43	12.80	4.93	Ependymal
Gabra5	gamma-aminobutyric acid (GABA) A receptor, subunit alpha 5	2.38	9.21	3.63	Ependymal
Prom1	prominin 1	2.04	94.88	43.61	NSC
Notch2	notch 2	1.52	3,043.79	1,871.60	NSC
Notch1	notch 1	1.39	130.37	87.75	NSC
Slc2a1 (GLUT1)	solute carrier family 2 (facilitated glucose transporter), member 1	1.23	603.62	460.45	Ependymal
Vcam1	vascular cell adhesion molecule 1	1.02	134.00	122.85	Ependymal
Notch3	notch 3	-1.13	211.48	223.76	NSC
Sox1	SRY (sex determining region Y)-box 1	-1.13	102.95	108.65	NSC
Vim	vimentin	-1.41	11,998.71	15,908.65	Ependymal
Hey1	hairy/enhancer-of-split related with YRPW motif 1	-1.60	1,222.26	1,830.69	Ependymal
Sox9	SRY (sex determining region Y)-box 9	-1.71	1,009.68	1,618.16	NSC
Bmi1	Bmi1 polycomb ring finger oncogene	-2.00	327.86	613.62	NSC
Cd24a	CD24a antigen	-2.12	623.28	1,240.93	Ependymal
Lrp2	low density lipoprotein receptor-related protein 2	-2.34	3.33	7.31	Ependymal
Sox2	SRY (sex determining region Y)-box 2	-2.43	524.67	1,192.50	NSC
Msi1	musashi RNA-binding protein 1	-2.86	16.73	44.88	NSC
Cd36	CD36 antigen	-3.36	15.87	49.99	Ependymal
Nes	nestin	-3.51	698.03	2,293.63	NSC
S100b	S100 protein, beta polypeptide, neural	-3.87	15.63	56.77	Ependymal
Foxj1	forkhead box J1	-4.11	133.33	513.18	Ependymal
Pax6	paired box 6	-4.34	21.05	85.57	NSC
Ecrg4	Esophageal cancer related gene 4	-11.01	34.04	351.12	NSC
Slc1a3 (GLAST)	solute carrier family 1 (glial high affinity glutamate transporter), member 3	-14.94	274.01	3,836.91	Ependymal

Fig. S4. Microarray analysis of gene expression in the β-gal+ VZ/SVZ and Ecrg4(+/-) cells

(A) Flow cytometry analysis of β-gal expression in the dissociated *ecrg4hetelo* VZ/SVZ cells and cultured Ecrg4(+/-) cells. (B) A list of the up- and down-regulated genes in the β-gal+ VZ/SVZ cells (fold change >1 and <-1).

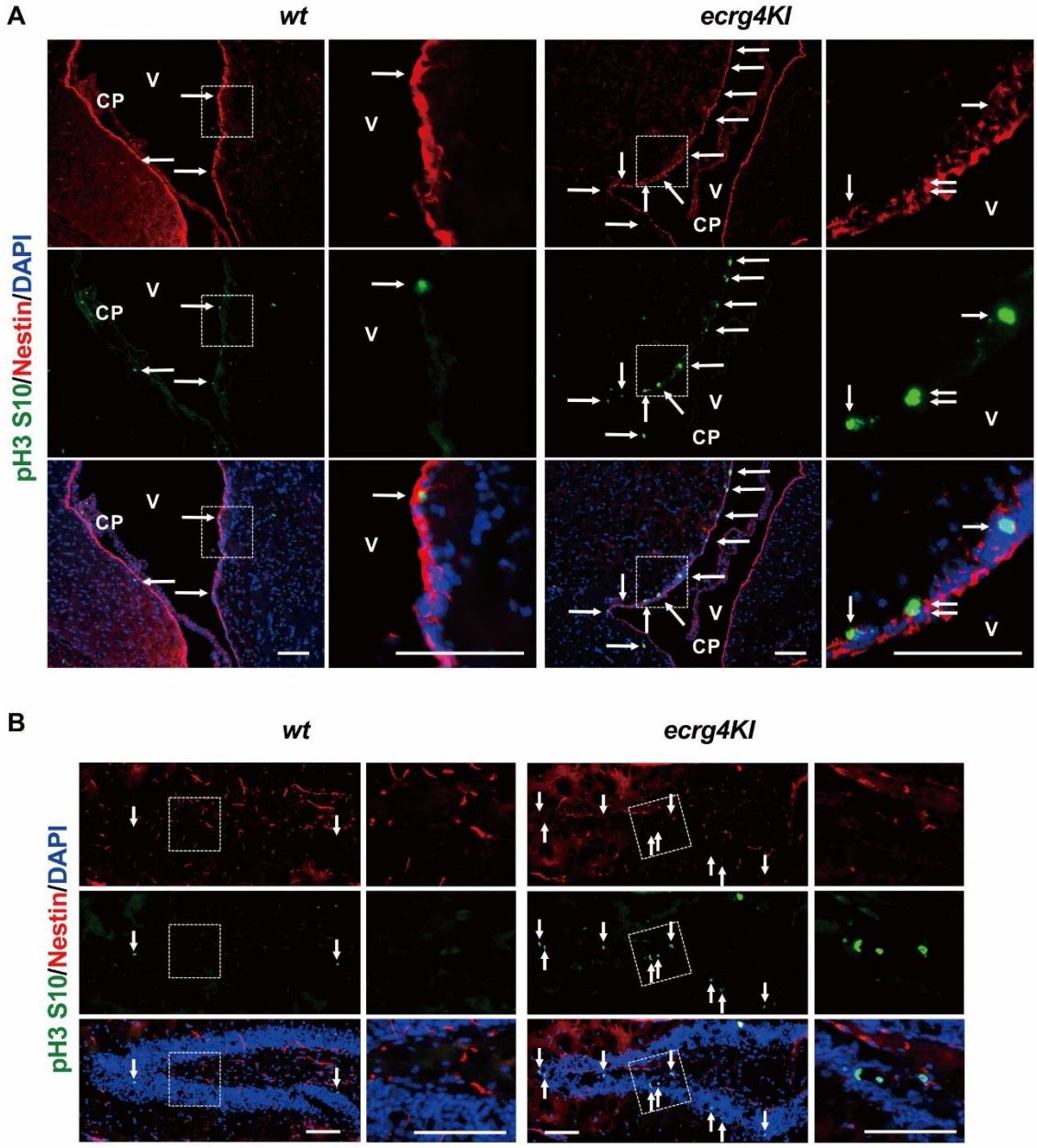

Fig. S5. Retention of proliferating cells in NSC niches of *Ecrg4KI* mice

Brain sections of *wt* and *ecrg4KI* were immunolabeled for pH3 S10 (green) and Nestin (red) to identify proliferating NSCs in VZ/SVZ (arrows in A) of 15m and DG (arrows in B) of 6m mice. Insets show high magnification images. All nuclei were counterstained with DAPI (blue). V: lateral ventricle. CP: choroid plexus. Scale, 200 μm.

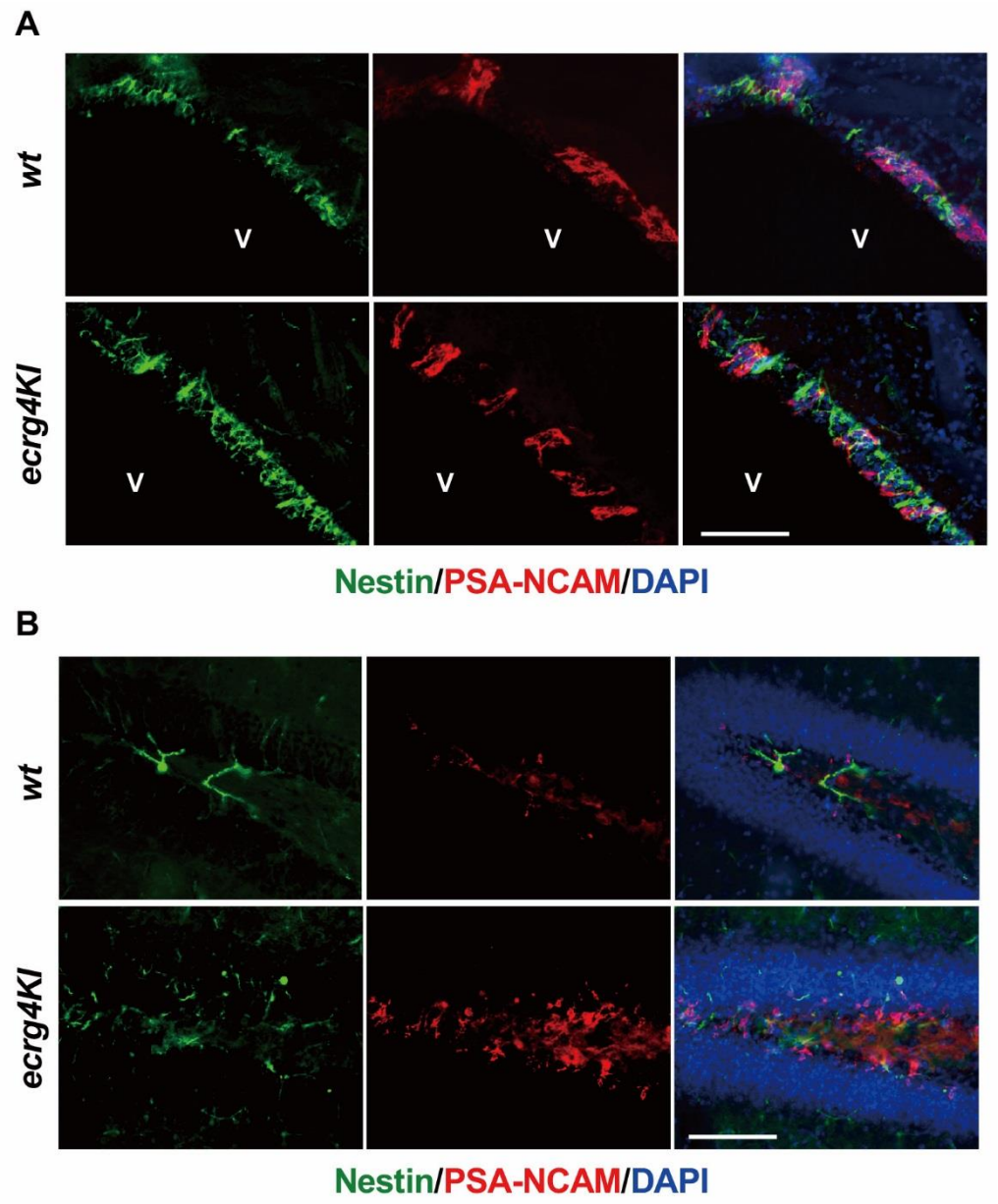

Fig. S6. Retention of neurogenesis in adult *Ecrg4KI* VZ/SVZ and DG

Brain sections of *wt* and *ecrg4KI* were immunolabeled for PSA-NCAM (green) and Nestin (red) to detect newly generated immature neurons in VZ/SVZ (A) and DG of 6m mice. All nuclei were counterstained with DAPI (blue). V: lateral ventricle. Scale, 200 μ m.

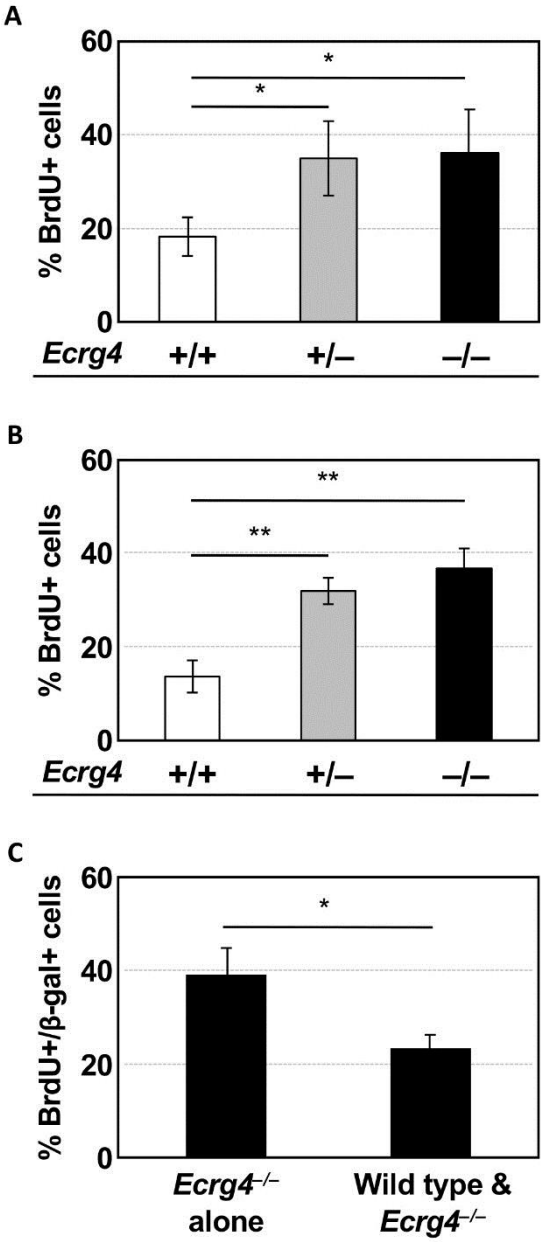

Fig. S7. Ecrg4 negatively regulates NSC proliferation

BrdU incorporation assay of Ecrg4(+/+), (+/-) and (-/-) cells that were prepared from *wt*, *ecrg4hetero*, and *ecrg4KI* 6m NSC niches, VZ/SVZ (A) and hippocampus (B), and cultured for 7 days. (C) BrdU incorporation assay of Ecrg4(-/-) cells that were cultured with or without Ecrg4(+/+) cells for 7 days. The proportion of BrdU-positive cells in β -gal+ cells is shown as the mean±SEM of three cultures. *p<0.05; **p<0.01.

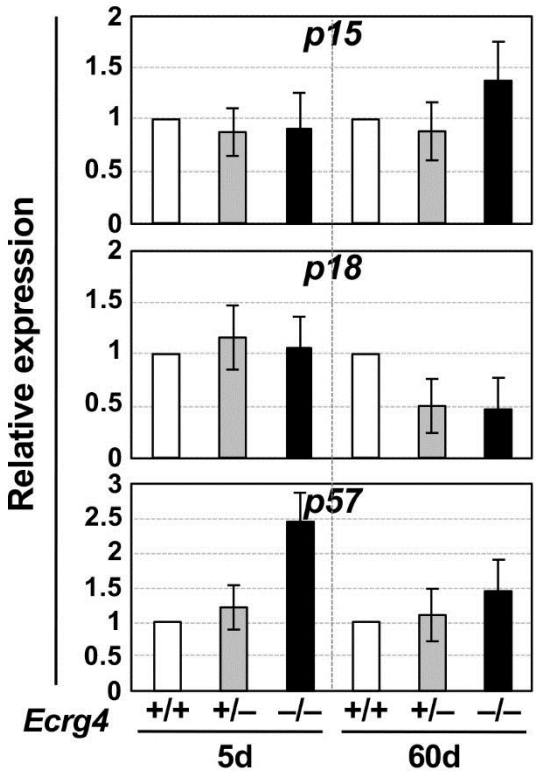

Fig. S8. Quantitative RT-PCR analysis of the expression of cdk inhibitors, *p15*, *p18*, and *p57*.

The expression of cdk inhibitors, *p15*, *p18*, and *p57* in Ecrg4(+/+), (+/-) and (-/-) cells, which were cultured for 5d and 60d, was analyzed by quantitative RT-PCR. The mRNA levels were shown as fold change over mRNA levels in Ecrg4(+/+) cells.

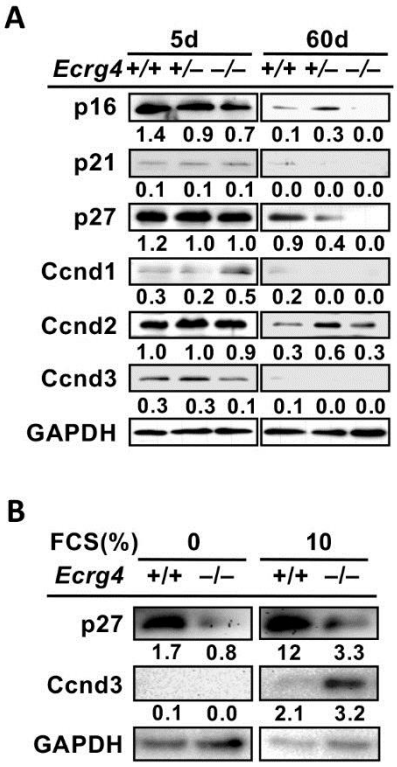

Fig. S9. Western blotting analysis of the expression of Cdk inhibitors and Ccnd1-3.

(A): Representative western blotting data of the expression of Cdk inhibitors, p16, p21 and p27, and Ccnd1-3 in Ecrg4(+/+), (+/-) and (-/-) cells that were cultured for 5d and 60d. (B): Representative western blotting data of the expression of p27 and Ccnd3 in Ecrg4(+/+) and (-/-) cells that were cultured in the presence of 0 and 10% FCS. GAPDH is a loading control. The intensity of the bands was measured by ImageJ software.

A

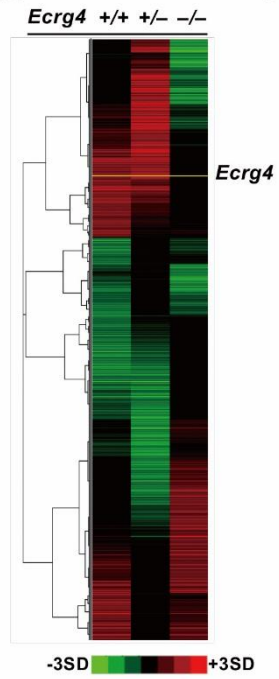

B

Gene Symbol	Description	Log2 ratio
Ddit4l	DNA-damage-inducible transcript 4-like	4.676
Sparcl1	SPARC-like 1 (mast9, hevin)	4.221
Six1	sine oculis-related homeobox 1 homolog	3.390
Foxg1	forkhead box G1	3.217
Tmem37	transmembrane protein 37	3.031
Gbp6	guanylate binding protein 6	2.974
Mup2	major urinary protein 2	2.911
F2rl2	coagulation factor II (thrombin) receptor-like 2	2.773
Tagln2	transgelin 2	2.654
Dbc1	deleted in bladder cancer 1 (human)	2.645
Nxph1	neurexophilin 1	2.485
Cd36	CD36 antigen	2.458
Abhd1	abhydrolase domain containing 1	2.406
Cadps	Ca^{2+} dependent activator protein for secretion	2.341
Slc7a4	solute carrier family 7, member 4	2.299
Apoa2	apolipoprotein A-II	2.241
Ccdc89	coiled-coil domain containing 89	2.218
Emb	embigin	2.141
Casp8	caspase 8	2.113
Ssm1b	RIKEN cDNA 2610305D13 gene	2.105
Ctsc	cathepsin C	2.037

C

Gene Symbol	Description	Log2 ratio
Ecrg4	Esophageal cancer related gene 4	-6.609
Eif2s3y	eukaryotic translation initiation factor 2, subunit 3, Y-linked	-5.129
Suhw2	suppressor of hairy wing homolog 2	-4.382
Cd82	CD82 antigen	-3.947
Fermt3	fermitin family homolog 3	-3.744
Acta2	actin, alpha 2, smooth muscle, aorta	-3.363
Mical1	microtubule associated monoxygenase, calponin and LIM domain containing 1	-2.926
Serpinh1	serine (or cysteine) peptidase inhibitor, clade H, member 1	-2.857
Gng2	guanine nucleotide binding protein (G protein), gamma 2 subunit	-2.831
Dhrs4	dehydrogenase/reductase (SDR family) member 4	-2.407
Tgfb1i1	transforming growth factor beta 1 induced transcript 1	-2.377
S100a10	S100 calcium binding protein A10 (calpactin)	-2.215
Ndrg1	N-myc downstream regulated gene 1	-2.164
Irx1	Iroquois related homeobox 1 (Drosophila)	-2.156
Foxb1	forkhead box B1	-2.054
Dbx2	developing brain homeobox 2	-2.043
Rab17	RAB17, member RAS oncogene family	-2.042
Rgs8	regulator of G-protein signaling 8	-2.041
Gas6	growth arrest specific 6	-2.014

Fig. S10. Microarray analysis of gene expression in Ecrg4(+/+), (+/-) and (-/-) cells

(A): Hierarchical clustering of Ecrg4(+/+), (+/-) and (-/-) cells using the TORAY 3D-gene Mouse Oligo Chip 24k. (B): A list of the up-regulated genes in Ecrg4(-/-) NSCs (Log2 ratio >2). (C): A list of the down-regulated genes in Ecrg4(-/-) cells (Log2 ratio <-2).

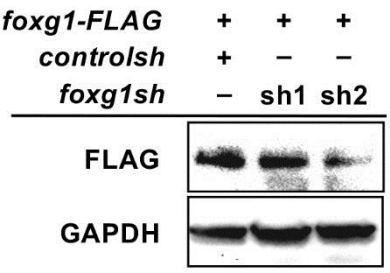

Fig. S11. Knockdown efficiency of *foxg1* shRNAs

FLAG-tagged mouse *foxg1* expression vectors were transfected with a *controlsh* or *foxg1sh* expression vectors into Cos7 cells. Cell extracts were harvested 2 d after transfection, and were analyzed by Western blotting using anti-FLAG and anti-GAPDH (loading control) antibodies.

Movies

Movie 1

This movie shows the Morris water maze analysis of wild-type mouse on Day1.

Movie 2

This movie shows the Morris water maze analysis of *ecrg4KI* mouse on Day1.

Movie 3

This movie shows the Morris water maze analysis of wild-type mouse on Day3.

Movie 4

This movie shows the Morris water maze analysis of *ecrg4KI* mouse on Day3.

Table S1. Primers used in this study

Gene name	Forward primer	Reverse primer
p15Ink4b	CCTGCCGGTAGACTTGGCTG	AACCCGCAGTCAATCTCCAG
p16Ink4a	TCTTGGTGAAGTTCGTGCGA	TTGCCCATCATCATCACCTG
p18Ink4c	AAGTGAGCTCTGCGAAGGAC	GCTCGGCCATTCTTTAGGGT
p19Arf	TCTTGGTGAAGTTCGTGCGA	TGCCCATCATCATCACCTGG
p21Cip1	CGGTGTCAGAGTCTAGGGGA	AGGATTGGACATGGTGCCTG
p27Kip1	ACTCTGAGGACCGGCATTTG	CTCATCCCTGGACACTGCTC
p57Kip2	GTAGCAGGAACCGGAGATGG	TTTACACCTTGGGACCAGCG
Six1	GCGATCACCTGCACAAGAAC	GGGTGATTGTGAGGCGAGAA
Foxg1	TTCCCAAGTCCTCGTTCAGC	TGATGATGGTGATGCTGGGG
Ddit4l	TGCCTCGGTTTACCCTTCAG	AAATGCTGGCCGGGTTCTTA
Irx1	CAACTACAGCGCCTTCTTGC	AATAAGCAGGCGTTGTGTGG
Ecrg4	AGCAGTGGTACCAGCAGTTC	CCAATGGCCGCATCTTCATC
18S	CGGACAGGATTGACAGATTG	CAAATCGCTCCACCAACTAA